Available online at www.sciencedirect.com
ScienceDirect
Polymer 49 (2008) 295–302
polymer
www.elsevier.com/locate/polymer

Combined effect of shear and fibrous fillers on orientation-induced crystallization in discontinuous aramid fiber/isotactic polypropylene composites

Boris Larin [a], Carlos A. Avila-Orta [b,c], Rajesh H. Somani [c], Benjamin S. Hsiao [c], Gad Marom [a,*]

[a] *Casali Institute of Applied Chemistry, The Institute of Chemistry, The Hebrew University of Jerusalem, Jerusalem 91904, Israel*
[b] *Departamento de Química de Polímeros, Centro de Investigación en Química Aplicada, Saltillo, Coahuila, C.P. 25100, Mexico*
[c] *Department of Chemistry, State University of New York at Stony Brook, Stony Brook, NY 11794-3400, USA*

Received 17 September 2007; received in revised form 21 October 2007; accepted 13 November 2007
Available online 17 November 2007

Abstract

The shear-induced crystallization behavior in isotactic polypropylene (iPP) composite melt containing short aramid fibers was investigated by means of WAXD (wide-angle X-ray diffraction) and SAXS (small-angle X-ray scattering) techniques using synchrotron radiation. The study was carried out in a post-shear isothermal crystallization mode at temperatures of 140–160 °C. Parameters pertaining to the crystallization morphology and kinetics were analyzed, including total crystallinity, orientated crystalline and amorphous fractions, dimensions of the formed shish–kebab structure, as well as induction time and rate of crystallization. The individual contributions of shear and fibers were evaluated and the combined effect was compared. The results clearly indicated that the effect is synergistic rather than additive.

Keywords: Shear; Shish–kebab crystallization; Aramid fiber

1. Introduction

The behavior of orientation-induced crystallization, caused by extensional or shear flow in polymer entangled melt, has been the subject of extensive study for many years [1]. Although shear is considered as a weaker flow than extensional, the shear-induced structural changes are very common in industrial processing (e.g., extrusion, injection molding) and have a profound impact on the resulting properties in final applications [2]. The subject of shear-induced crystallization is particularly relevant in controlling the properties of semi-crystalline polymers. In the early stages of crystallization, a scaffold of 'shish–kebabs' has been reported in entangled melt (using polyethylene as a model system [3]) and this scaffold appears to act as a precursor structure to induce full scale crystallization at low temperatures.

The application of shear is clearly sufficient to stretch and align some polymer chains, allowing them to form orientated crystalline structures (shish–kebabs) that can eventually develop into orientated crystalline domains [4]. This behavior is a function of several factors, including processing conditions (e.g., temperature, deformation rate, and deformation strain) and polymer properties (e.g., molecular weight and distribution). During the shish–kebab formation, the shish develops first from extended chains, which can be viewed as primary nuclei to anchor the folded chain crystallites (kebabs) that induce lateral lamellar growth. The phenomenon of shear-induced shish–kebab structure in isotactic polypropylene (iPP) has been studied quite extensively by this group, considering both processing and material variables [5–11]. The results can be explained by the concept of critical orientation molecular weight and the relaxation time spectrum of the deformed polymer chains [9,10].

* Corresponding author. Tel.: +972 2 658 5898; fax: +972 2 658 6068.
E-mail address: gadm@vms.huji.ac.il (G. Marom).

0032-3861/$ - see front matter © 2007 Elsevier Ltd. All rights reserved.
doi:10.1016/j.polymer.2007.11.024

In recent studies, we examined the shear-induced crystallization behavior in iPP reinforced by acicular inclusions, such as short aramid fibers and carbon nanotubes. The premise of these studies was that, in addition to the shear flow that promotes chain stretching, disentanglement, and alignment, orientation of the acicular inclusions parallel to the flow lines would also occur [12]. Thereafter, both the aligned and the stretched polymer chains (at the atomistic level) and the fibers (at microscopic scale) could generate orientated crystalline morphology involving folded chain crystallization. In the latter, the phenomenon is termed transcrystallization, which has been widely reported in fiber-reinforced composites when the matrix is crystallizable. The combined effect has recently been reported in the system based on microfibrillar PET/PP blend [13]. Our group also confirmed this behavior in shear-induced crystallization studies involving a materials' system of iPP matrix and ultrahigh molecular weight polyethylene (UHMWPE) fibers, where the shish–kebab structure was further enhanced by the presence of UHMWPE fibers and formed highly orientated cylindritic morphology [14,15].

In another study, shear-induced crystallization behavior in carbon nanotube-reinforced iPP nanocomposite was investigated. The results showed a significant improvement of the overall crystallization kinetics and total crystallinity compared to unfilled systems. However, the presence of the nanotubes was found to decrease the fraction of orientated crystals as a result of the strong nucleating effect of un-orientated nanotubes [16]. It is apparent that shear-induced orientation of acicular inclusions depends on their aspect ratio. In nanocomposites, the effective aspect ratio of the fillers depends on the final aggregation state resulting from the material processing.

In a preceding study on chopped aramid fiber-reinforced iPP, the presence of fibers was found to enhance the behavior of shear-induced crystallization as well as the overall orientation of the matrix [17]. The observation indicated two types of crystal growths, one from the induced shish structure appearing almost immediately after the application of shear and the other from the surface of embedded aramid fibers. The first process led to the development of the kebab morphology, whereas the latter process resulted in the formation of transcrystalline structure.

The aim of the current study was to quantitatively evaluate the combined effect of these two simultaneously occurring crystallization pathways, namely from the shear-induced shish assemblies and from the embedded and axially aligned fibers. The chosen experimental conditions involved *in situ* small-angle X-ray scattering (SAXS) and wide-angle X-ray diffraction (WAXD) measurements of aramid fiber-reinforced iPP melts under shear flow. Specifically, the molten iPP composites were subjected to shear at different temperatures (140–160 °C) followed by isothermal crystallization for 1 h, during which time-resolved X-ray images were collected. The data were analyzed to follow the morphological and crystalline changes in real time, including nucleation induction time, crystallization kinetics, level of crystalline and/or amorphous orientation, and degree of crystallinity. A particular objective of the study was to determine whether the combined effect was additive or synergistic.

2. Experimental

2.1. Materials and sample preparation

Melt-mixed short fiber-reinforced polymer composite samples based on isotactic polypropylene (iPP; Capilene U77, Carmel Olefins, Israel, high flow, nucleated homopolymer, having an average molecular weight, M_w, of 135,000 g/mol) and chopped aramid fibers (AF; Kevlar 49, DuPont) of 3.2 mm length (considering a fiber diameter of 14 μm and the aspect ratio of 228) were prepared using the following procedures. Mechanical blending of iPP with 5 wt% chopped fibers (iPP/AF) was carried out in a batch laboratory twin-screw microcompounder (DSM) with recirculation facility at 190 °C in two consecutive 10 min cycles, with screw speed 100 rpm. Antioxidant (0.1% w/w; Irganox B-225) was added to prevent polymer degradation at high temperatures. The resulting blends were pressed in a mold to produce 0.5–0.7 mm thick films, from which ring specimens with internal diameter of 10 mm and external diameter of 20 mm were punched out for the shear X-ray testing.

2.2. In situ X-ray study of samples under shear

A Linkam CSS-450 shearing apparatus was used to carry out the shear X-ray measurements. The apparatus consisted of two circular parallel plates (one stationary and the other rotated by a stepping motor) and two X-ray windows (diamond and Kapton), to allow *in situ* X-ray scattering/diffraction measurements. The temperature profile was precisely controlled by heating and cooling modules to an accuracy of ±0.2 °C. The ring-shaped sample was sandwiched between two parallel plates of the apparatus, heated quickly to 200 °C and held at this temperature for 5 min to delete the crystalline history, followed by rapid cooling to varying experimental temperatures (140–160 °C), where shear was imposed at a rate of 60 s^{-1} for 5 s. The sheared melt was allowed to isothermally crystallize for 1.0 h and then cooled to room temperature at a rate of 30 °C/min.

In situ WAXD and SAXS measurements were performed at Beamline X27C, in the National Synchrotron Light Source (NSLS), Brookhaven National Laboratory (BNL), Upton, NY, USA. The details of the experimental conditions and setup have been described previously [18]. The chosen X-ray wavelength was 1.371 Å. For WAXD measurements, the sample to detector distance was 120.5 mm determined by aluminum oxide (Al_2O_3) as a standard. For SAXS measurements, the sample to detector distance was 1820.2 mm determined by silver behenate as a standard. In both X-ray measurements, a CCD X-ray detector (MAR, USA) with a pixel size of 158 μm was used to collect the data. The collected 2D images were further corrected for air scattering and beam fluctuations.

2.3. X-ray data analysis

The WAXD scattered intensity (analyzed using the Polar software, Stonybrook Technology and Applied Research Inc., NY, USA) from a partially orientated sample (see example

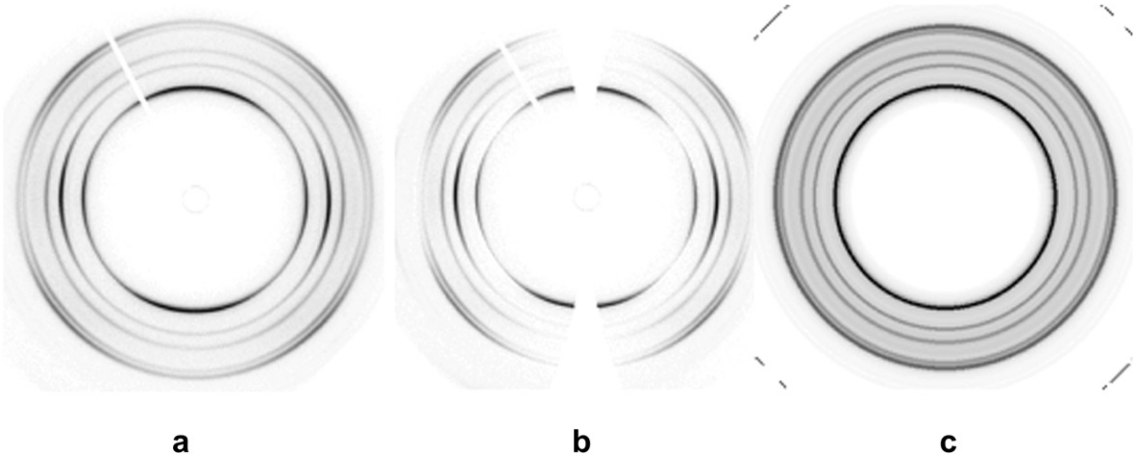

Fig. 1. (a) Typical diffraction pattern of iPP/AF at 150 °C after 1 h, divided by the Polar program to (b) orientated and (c) un-orientated fractions.

in Fig. 1) usually contains two contributions: (1) the isotropic part due to the amorphous phase and un-orientated crystals and (2) the anisotropic part due to the orientated crystals. The total crystallinity thus can be separated into two fractions due to un-orientated and orientated crystals. To accomplish this, the total scattering was first deconvoluted into contributions from orientated and un-orientated parts, using the "halo" method described earlier [19] (as seen in Fig. 1).

The 1D intensity profiles of orientated and isotropic fractions were integrated from the corresponding 2D deconvoluted patterns. Representative results from the sheared iPP/aramid fiber composite after 1 h isothermal crystallization are illustrated in Fig. 2, where total, orientated and isotropic 1D intensity profiles are shown. The crystalline and amorphous contributions of orientated and isotropic fractions were obtained from the integrated intensity profiles using the 1D peak deconvolution method [6]. The orientated fraction consists of orientated crystalline phase and orientated amorphous phase, while the isotropic fraction consists of isotropic crystalline phase and isotropic amorphous phase. The quantity of crystalline and amorphous fraction was further calculated using a peak fit program (EVA software).

From the SAXS images, two parameters were estimated, i.e., the domain size (or the lateral dimension of the lamellae),

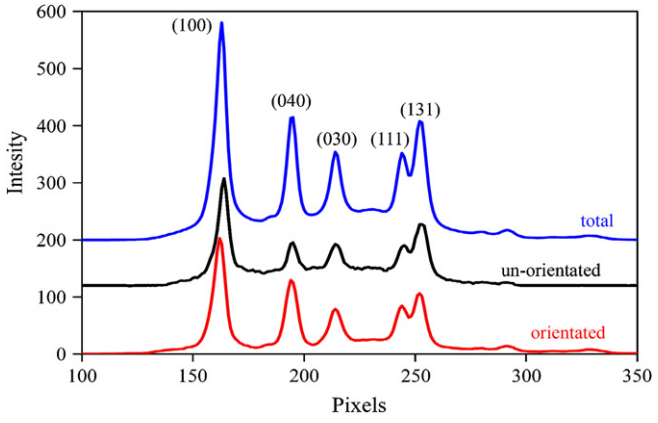

Fig. 2. Integrated WAXD profiles of total, orientated, and isotropic crystallinity of iPP/AF-S composite isothermally crystallized at 150 °C.

D, and the long period (the average spacing between adjacent lamellae), $L = 2\pi/q_{max}$, where q_{max} is the position of scattering maximum). D was calculated from $D = (8\pi/w)^{0.5}$ where w is peak width at half height.

2.4. Characterization of post-sheared samples

The sheared samples were etched following Bassett's procedure to enhance the crystalline structure [20]. The etched specimens were coated with Au–Pd using the SC7640 Sputter. Scanning electron microscopic (SEM) measurements were carried out with a high resolution electron microscope (HRSEM, FEI Sirion) operated at 10 kV. Thermal analysis was carried out in a heating–cooling–heating cycle (25–200–25–200 °C) (Mettler DCS-30 calorimeter) at a heating/cooling rate of 10 K/min^{-1} under nitrogen. The degree of crystallinity and the melting points were obtained from the first heating interval.

3. Results

3.1. Orientated crystallization

In the first part of this study, *in situ* WAXD experiments were carried out to generate crystallographic and kinetic data on four different systems, i.e., neat iPP, sheared iPP (iPP-S), iPP/AF composites, and sheared iPP/AF composites (iPP/AF-S). Representative synchrotron WAXD intensity profiles of iPP/AF-S taken at different crystallization times and temperatures are shown in Fig. 3. All observed diffraction profiles indicate the presence of an iPP α phase [21,22]. At time zero, the data exhibit a diffuse scattering feature without noticeable crystalline reflections, which is consistent with the presence of an amorphous melt. The gradual appearance of diffraction rings indicates the growth of crystallinity; the enhanced variation of azimuthal intensity in all reflections indicates the increase in crystalline orientation (e.g., the initial ring-like feature is replaced by diffraction arcs at the later stage). The data in Fig. 3 confirm that orientated crystallization took place at all experimental temperatures. At 140 °C the kinetics of crystallization appeared to have the highest rate, while the best crystal

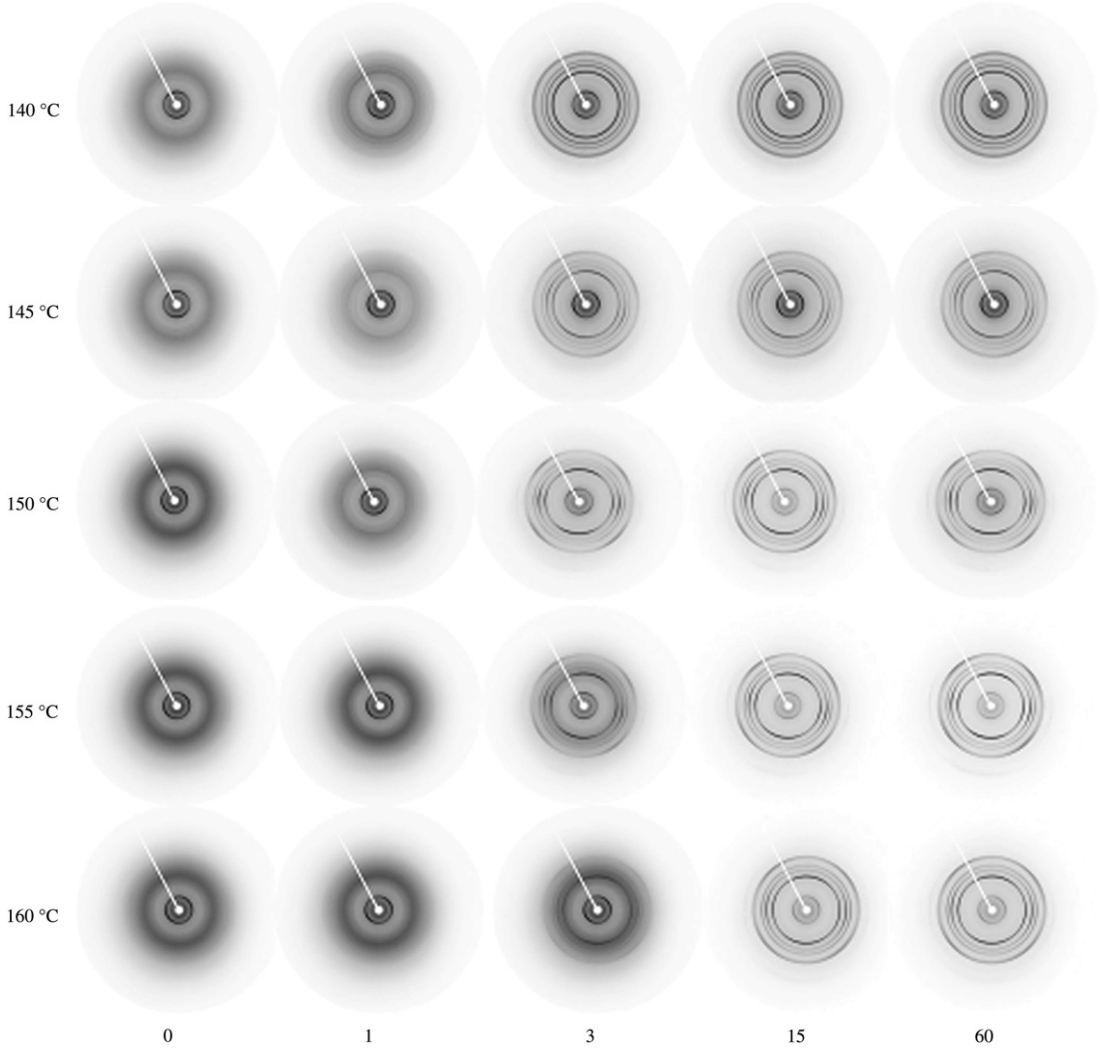

Fig. 3. 2D WAXD images of iPP/AF-S composites collected at selected times during 1 h isothermal crystallization at different experimental temperatures.

orientation was obtained at 150 °C. Contrary to our previous studies on other iPP systems, the chosen iPP matrix contained a commercial nucleating agent. However, its nucleating effect is not noticeable compared to the dominant effects of shear and fibers.

The results in Fig. 3 are representative for all the samples of iPP and iPP/AF with and without shear, from which an extensive database was generated. Detailed analyses of this database produced quantitative results that are summarized in Table 1 (results from DSC were also included). This table maps the scope of the study by presenting the experimental array and the basic data of the degree of crystallinity and melting point as determined from WAXD and DSC of the room temperature (RT) structures and of *in situ* measurements after 1 h at the experimental temperature. It was seen that WAXD and DSC methods yielded comparable values of crystallinity from samples cooled to room temperature. In general the degree of crystallinity on the basis of WAXD is higher than the corresponding DSC value. This is attributed in the literature to the contribution in WAXD of crystalline–amorphous transition layers or dense rigid amorphous material inbetween the lamellar crystal grains – not counted for by DSC [23].

Considering the effects of shear and fibers, it is seen from Table 1 that both factors positively increase the degree of RT crystallinity (e.g., the WAXD data at 150 °C) by 3 and 1%, respectively, where the combined effect increases the degree of RT crystallinity by 6%. A similar behavior was also observed in the *in situ* crystallinity (with the corresponding degree of crystallinity changes of 2, 2, and 7%) after 1 h at the experimental temperature. It is apparent that as temperature increases, this phenomenon becomes more prominent, since little crystallization can take place without shear. For example, at 155 °C the *in situ* crystallinity after 1 h is only 8% for un-sheared iPP, but becomes 18, 16, and 33% as a result of the shear, fibers, and combined effect, respectively. On the other hand, the change of melting point is inconclusive, except for a distinctively sharp rise in all the iPP/AF-S samples.

Analysis of the WAXD data produces values of an orientated fraction. These values as a function of temperature for the iPP-S and iPP/AF-S samples after isothermal crystallization for 1 h are summarized in Fig. 4. It is seen that a crystallization temperature of 150 °C produces the highest value of orientated fraction, which due to the fibers increases from around 30% to more than 50%, which is consistent with the

Table 1
Degree of crystallinity and the melting point from post-sheared samples at crystallization temperature and room temperature

Temperature (°C)	Sample	T_m (°C)	% Crystallinity WAXD at 60 min	% Crystallinity WAXD at RT	% Crystallinity DSC at RT
140	iPP	166.71	42.65	49.88	48.96
	iPP-S	165.87	41.56	48.12	47.15
	iPP/AF	167.12	44.05	51.1	49.35
	iPP/AF-S	167.32	46.86	55.2	50.61
145	iPP	165.86	40.38	49.99	47.95
	iPP-S	165.13	41.43	51.5	50.80
	iPP/AF	165.89	40.93	50.91	48.1
	iPP/AF-S	170.75	42.14	54.3	52.17
150	iPP	167.45	36.81	48.31	44.18
	iPP-S	168.39	39.19	51.12	48.52
	iPP/AF	168.85	39.01	49.08	48.04
	iPP/AF-S	170.2	43.92	54.23	51.57
155	iPP	165.71	7.76	49.29	43.52
	iPP-S	164.88	25.11	50.34	43.95
	iPP/AF	167.84	23.42	52.14	45.95
	iPP/AF-S	169.47	40.85	55.15	48.92
160	iPP	166.06	–	–	43.22
	iPP-S	166.98	–	–	44.69
	iPP/AF	164.98	4.52	42.78	39.80
	iPP/AF-S	172.57	39.87	57.18	47.70

qualitative observation shown in Fig. 3. An optimal temperature of 150 °C for shear-induced crystallization of iPP/AF-S samples has been identified. Below 150 °C, the viscosity of the melt is too high for effective shear contribution, whereas above 150 °C, the stretched chains relax before the effective nucleation process can occur.

Both values of orientated and un-orientated degrees of crystallinity were calculated (based on the component separation procedure described in Fig. 2) and the results are summarized in Table 2. Again, it is found that the combined effect of shear and fibers is significantly greater than the sum of individual effects. It is seen that the application of shear increases the degree of orientated crystallinity by some 8 points (from 5.9 to 14.3%), the inclusion of fibers increases that value by less than 1 point, while the combined effect increases the degree of orientated crystallinity by 20 points (from 5.9 to 25.9%).

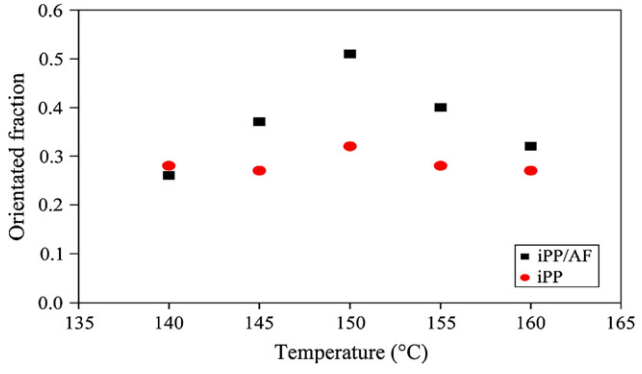

Fig. 4. The quantity of orientated fraction in pure iPP and in iPP/AF sheared composites at different crystallization temperatures.

Table 2
Values of orientated and un-orientated degrees of crystallinity after isothermal crystallization at 150 °C

	Orientated crystallinity	Un-orientated crystallinity
iPP	5.9	30.4
iPP-S	14.3	25.2
iPP/AF	6.6	33.9
iPP/AF-S	25.9	16.3

The kinetics of crystallization was tracked by monitoring the degree of crystallinity as a function of post-shear time; results from the 150 °C experiment are illustrated in Fig. 5. It is seen that under the combined effect of shear and fibers the maximum degree of crystallinity is obtained within 5 min compared with incomplete crystallization even after 60 min of annealing for the control iPP sample. Also apparent is the significantly stronger effect of the fibers compared with that of shear (20 and 40 min, respectively). Furthermore, the crystallization traces in Fig. 5 also allow us to compare the induction times for nucleation, the results of which are presented by a bar diagram in Fig. 6. The results obtained at 150 °C indicate that the induction time was shortened by 14 and 11 min due to the individual effects of shear and fibers, respectively, and by 16 min due to the combined effect. Regarding the rate of crystallization (expressed by the linear regression determined slope of the linear portion of the crystallization curve), the results in Fig. 6 produce the values of 7.4, 15.4, 24.1, and 125.4×10^{-3} min^{-1} for the iPP, iPP-S, iPP/AF, and iPP/AF-S samples, respectively. Clearly, while the net effect of either shear or fibers can double or triple the crystallization rate, their combined effect is 17-fold.

3.2. Structural evolution

The evolution of lamellar morphology in iPP-S and iPP/AF-S samples was studied by *in situ* SAXS technique during isothermal crystallization for 1 h. Only sheared samples were monitored because quiescent crystallization of iPP and iPP/AF samples did not exhibit any distinctive SAXS images. A series of time-resolved 2D SAXS images of iPP/AF-S samples during isothermal crystallization at different temperatures are illustrated in Fig. 7. The time-zero images at different temperatures always indicate the completely amorphous structure.

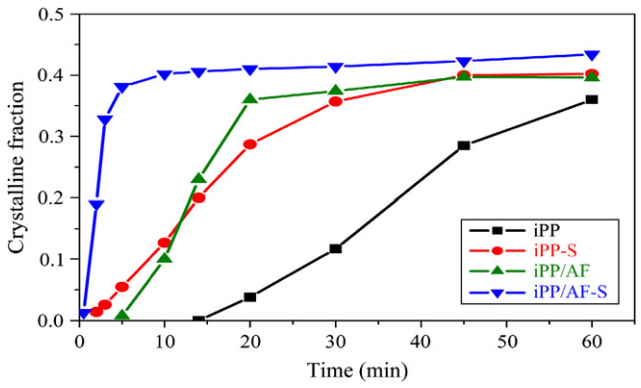

Fig. 5. Crystalline fraction evolution for samples prepared at 150 °C.

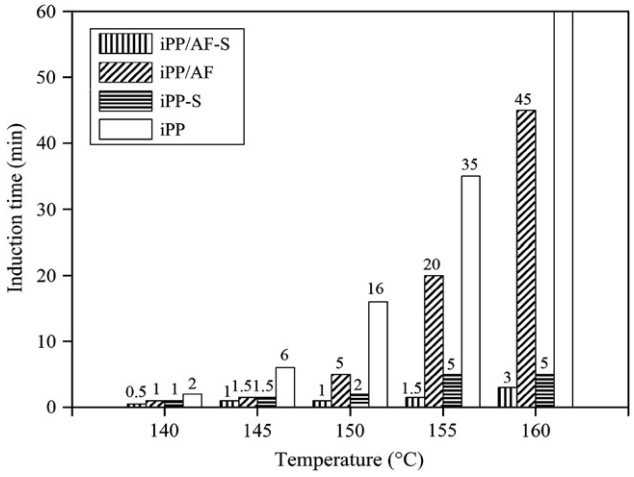

Fig. 6. Induction times for iPP crystallization at different temperatures.

However, a pair of meridian maxima forms immediately after the shear, attesting to the formation of orientated lamellar kebabs (induced by the shish) and/or transcrystalline structure (induced by the fibers) aligned perpendicular to the flow direction. It is also seen that at 150 °C, the meridian maxima emerge at shorter times than that at 155 °C. In addition, the intense isotropic ring at 150 °C, which indicates the formation of unorientated crystals, is also weaker than that at 145 °C. These findings are in agreement with the WAXD results, showing the maximum orientation at 150 °C. The equatorial streaks (indicative of the shish formation at the early stages of the nucleation process) were observed only in the iPP-S samples.

From SAXS results, two parameters were estimated, namely, D − the domain size or the lateral dimension of the crystal lamellae and L − the long period or the average spacing between adjacent lamellae. In pure iPP-S and iPP/AF-S samples at 150 °C, the L value decreases but the D value increases sharply (it reaches a plateau at around 10 min). This is shown for the iPP/AF-S sample in Fig. 8. The comparison of the respective plateau values for the iPP-S and iPP/AF-S samples is $L = 29$ and 34 nm, and $D = 19$ and 23 nm, respectively. These results, indicating that the presence of fiber can increase both interlamellar spacing and lateral lamellar diameter, can be attributed to the development of transcrystalline layer at the fiber surface.

3.3. Morphological observations

SEM examinations of etched surfaces from the sheared composite samples provide important morphological information on the lamellar orientation in both bulk and fiber interfacial crystalline domains. Although the main purpose of this investigation was to analyze the morphology of the matrix in the vicinity of the fiber surface, the effect of shear on the bulk morphology of the matrix was clearly seen [17]. A micrograph of two fibers and of the iPP matrix at the vicinity of the aramid fiber surface is shown in Fig. 9. Two types of morphology were seen near the interface: one resembled the familiar transcrystalline structure with lamellae growing perpendicular to the fiber direction and the other exhibited the shish−kebab morphology. We consider that only a small fraction of the fiber surface has been exposed by the etching treatment; it is clear that most of the matrix volume was taken by transcrystallinity, while the shish−kebab morphology was pushed toward the boundaries of the transcrystalline layer. This indicates that the effect of transcrystallization (from the fiber surface) is more profound than that of shish−kebab formation. This is reasonable as the chosen shear condition is relatively weak; this conclusion is also consistent with the SAXS results also showing the dominant transcrystallization effect.

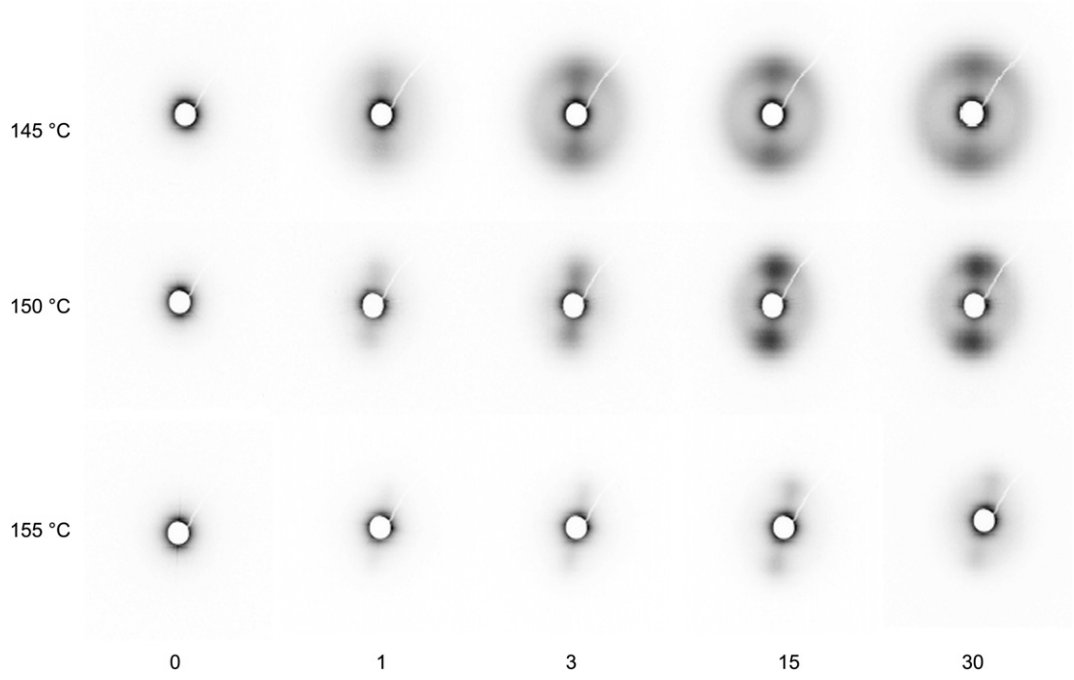

Fig. 7. 2D SAXS images of iPP/AF-S composites collected at selected times during first 30 min of isothermal crystallization at 145−155 °C.

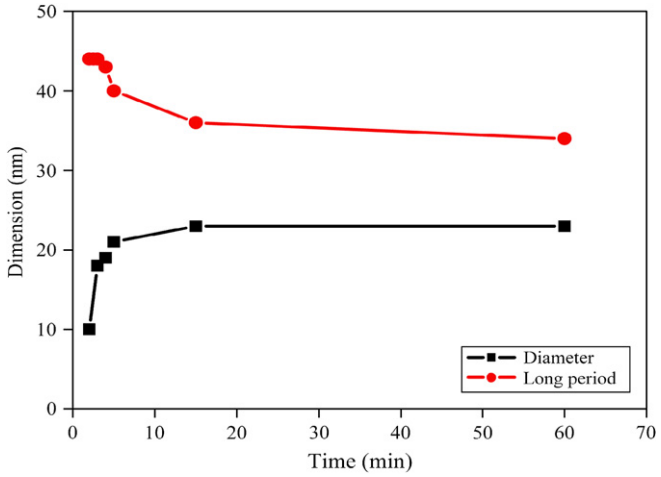

Fig. 8. The changes in the diameter of the lamellar disc and the long period with time for iPP/AF-S samples prepared at 150 °C.

4. Discussion

In this section, we determine the nature of the interactions between the individual effects of applied shear and embedded fibers and the synergy of the combined effect. Based on our preliminary research on an identical system at a single temperature of 145 °C and with regard to qualitative observations of the resultant nucleating effect of the two components (shear and fibers), we initially hypothesized that the effect (manifested by an extremely short crystallization time of 3 min) was additive [17]. However, judging by a wide range of quantitative parameters measured in this work, we positively recognize the synergy between the application of shear and the inclusion of short fibers. This is because the combined effect of shear and fibers significantly enhances the crystallization kinetics and the crystal orientation when compared to the sum of individual effects. The measured parameters included the total degree of crystallinity, the fractions of the orientated and un-orientated crystalline phases, as well as the nucleation and crystallization rates.

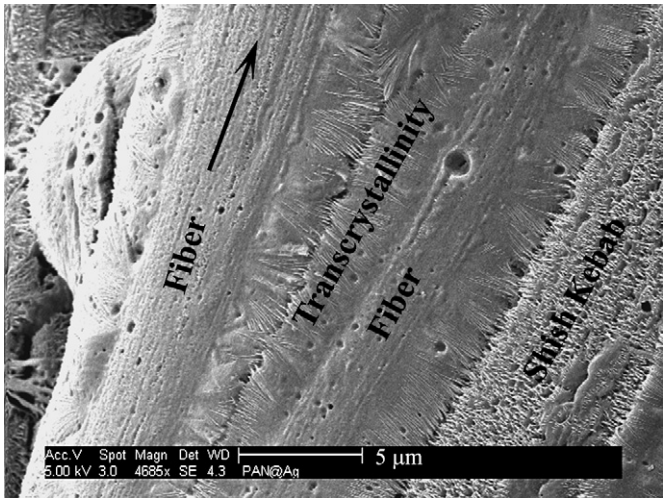

Fig. 9. High resolution SEM image of an etched tapered cross-section, showing an example of exposed fibers and of the iPP matrix and two types of morphologies at the vicinity of its surface. The arrow marks the shear direction.

We propose that the source of the synergy is due to the interfacial interactions between the shear-aligned fibers and the orientation and stretching of polymer chains. In an analogy to an earlier study by our groups [14], in which the presence of immiscible orientated UHMWPE domains (that originated from molten PE fibers) could facilitate the crystallization kinetics of the surrounding iPP matrix, we offer the following explanation. The fiber surface may provide pinning points to the surrounding iPP chains which would increase their effective relaxation times. Such anchoring interactions can lead to the retention of the molecular stretching and orientation after flow, thus creating more shish structures and promoting the kebab (lamellar) growth perpendicular to the fiber axis. In other words, nucleation of iPP is probably enhanced at the surface of the aramid fiber by a high concentration of stretched chains. This effect of the fiber seems similar to the effect of long chains in polymer under flow – even of a different polymer additive [15]. Thus, the excessive nucleation process induced by fiber surface interactions through transcrystallization, in addition to the typical shish–kebab formation induced by flow under shear, may account for the synergistic effect.

5. Conclusions

The quantitative crystallization and morphological parameters obtained from real time WAXD measurements, including the total degree of crystallinity, the degree of crystallinity of the orientated phase, and the nucleation and crystallization rates, present a clear picture of synergy between the shear and the fiber contributions. Their combined effect is significantly larger than the arithmetic sum of their individual effects, namely, the changes induced by shear compared to the quiescent iPP and by fiber reinforcement compared to the neat iPP. The SAXS and SEM observations suggest that the source of the synergistic effect is an additional new crystallization role performed by the stretched chains on the fiber surface. This generates a high concentration of shish nuclei at the fiber surface on top of the nucleation sites due to transcrystallization.

Acknowledgements

The research of the Israeli authors was supported by the Israel Science Foundation (Grant no. 69/05). The assistance in WAXD data analysis of Dr. Vladimir Uvarov from the Unit for Nanoscopic Characterization of the Hebrew University of Jerusalem is thankfully acknowledged. The US team thanks the financial support of the National Science Foundation (DMR-0405432).

References

[1] Schultz JM. Polymer crystallization. New York: Oxford University Press; 2001 [chapter 6].

[2] Fujiyama M. In: Karger-Korkis J, editor. Higher order structure of injection-molded polypropylene. Polypropylene, vol. 1. UK: Chapman and Hall; 1995 [chapter 6].
[3] Pennings AJ, Keil AM. Colloid Polym Sci 1965;205: 160–2.
[4] Yamazaki S, Watanabe K, Okada K, Yamada K, Tagashira K, Toda A, et al. Polymer 2005;46:1675–84.
[5] Somani RH, Hsiao BS, Nogales A, Srinivas S, Tsou AH, Sics I, et al. Macromolecules 2000;33:9385–94.
[6] Somani RH, Yang L, Hsiao BS, Fruitwala H. J Macromol Sci Phys 2003;B42:515–31.
[7] Somani RH, Yang L, Hsiao BS, Agarwal PK, Fruitwala H, Tsou A. Macromolecules 2002;35:9096–104.
[8] Somani RH, Yang L, Hsiao BS. Physica 2002;A304:145–7.
[9] Somani RH, Hsiao BS, Nogales A, Fruitwala H, Srinivas S, Tsou A. Macromolecules 2001;34:5902–9.
[10] Nogales A, Hsiao BS, Somani RH, Srinivas S, Tsou AH, Balta-Calleja FJ, et al. Polymer 2001;42:5247–56.
[11] Agarwal PK, Somani RH, Weng W, Mehta A, Yang L, Ran S, et al. Macromolecules 2003;36:5226–35.
[12] Folkes MJ, Russell DA. Polymer 1980;21:1252–8.
[13] Li ZM, Li LB, Shen KZ, Yang W, Huang R, Yang MB. Macromol Rapid Commun 2004;25:553–8.
[14] Dikovsky D, Marom G, Avila-Orta CA, Somani RH, Hsiao BS. Polymer 2005;46:3096–104.
[15] Avilla-Orta CA, Burger C, Somani RH, Yang L, Marom G, Medelline-Rodrigues FJ, et al. Polymer 2005;46:8859–71.
[16] Kelarakis A, Yoon K, Sics I, Somani RH, Chen X, Hsiao BS, et al. J Macromol Sci Phys 2006;45:247–61.
[17] Larin B, Marom G, Avila-Orta CA, Somani RH, Hsiao BS. J Appl Polym Sci 2005;98:1113–8.
[18] Yang L, Somani RH, Sics I, Hsiao BS, Kolb R, Fruitwala H, et al. Macromolecules 2004;37:4845–59.
[19] Ran S, Zong X, Fang D, Hsiao BS, Chu B. J Appl Crystallogr 2000;33:1031–6.
[20] Bassett DC, Hodge AM. Proc R Soc London 1981;A377:25–37.
[21] Dean DM, Rebenfeld L, Register RA, Hsiao BS. J Mater Sci 1998;33: 4797–812.
[22] Assouline E, Wachtel E, Grigull S, Lustiger A, Wagner HD, Marom G. Polymer 2001;42:6231–7.
[23] Homminga DS, Goderis B, Mathot VBF, Groeninckx G. Polymer 2006;47:1630–9.